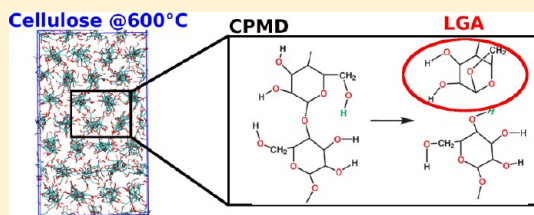


Ab Initio Dynamics of Cellulose Pyrolysis: Nascent Decomposition Pathways at 327 and 600 °C

Vishal Agarwal,^{†,§} Paul J. Dauenhauer,[‡] George W. Huber,^{‡,||} and Scott M. Auerbach^{*,‡}[†]Department of Chemical Engineering and [‡]Department of Chemistry, University of Massachusetts, Amherst, Massachusetts 01003, United States

S Supporting Information

ABSTRACT: We modeled nascent decomposition processes in cellulose pyrolysis at 327 and 600 °C using Car–Parrinello molecular dynamics (CPMD) simulations with rare events accelerated with the metadynamics method. We used a simulation cell comprised of two unit cells of cellulose I β periodically repeated in three dimensions to mimic the solid cellulose. To obtain initial conditions at reasonable densities, we extracted coordinates from larger classical NPT simulations at the target temperatures. CPMD-metadynamics implemented with various sets of collective variables, such as coordination numbers of the glycosidic oxygen, yielded a variety of chemical reactions such as depolymerization, fragmentation, ring opening, and ring contraction. These reactions yielded precursors to levoglucosan (LGA)—the major product of pyrolysis—and also to minor products such as 5-hydroxy-methylfurfural (HMF) and formic acid. At 327 °C, we found that depolymerization via ring contraction of the glucopyranose ring to the glucofuranose ring occurs with the lowest free-energy barrier (20 kcal/mol). We suggest that this process is key for formation of liquid intermediate cellulose, observed experimentally above 260 °C. At 600 °C, we found that a precursor to LGA (pre-LGA) forms with a free-energy barrier of 36 kcal/mol via an intermediate/transition state stabilized by anchimeric assistance and hydrogen bonding. Conformational freedom provided by expansion of the cellulose matrix at 600 °C was found to be crucial for formation of pre-LGA. We performed several comparison calculations to gauge the accuracy of CPMD-metadynamics barriers with respect to basis set and level of theory. We found that free-energy barriers at 600 °C are in the order pre-LGA < pre-HMF < formic acid, explaining why LGA is the kinetically favored product of fast cellulose pyrolysis.



1. INTRODUCTION

Research efforts have recently intensified to find viable pathways for unlocking the vast energy reserves in lignocellulosic biomass.¹ Fast pyrolysis of lignocellulosic biomass, which involves rapid heating in the absence of oxygen,^{2–4} is one of the most promising approaches for renewable production of liquid transportation fuels.^{5–7} Cellulose pyrolysis has been under study for more than 6 decades;⁸ despite this effort, the molecular-level processes underlying pyrolysis remain poorly understood.⁹ More than 50% of plant matter comprises cellulose;¹⁰ understanding cellulose pyrolysis chemistry is thus crucial for developing efficient biofuel production technologies. In the present article, we addressed this issue by revealing nascent decomposition reaction pathways of cellulose using Car–Parrinello molecular dynamics (CPMD).¹¹

Cellulose pyrolysis is a complex process involving myriad coupled reaction pathways. Most of the experimental literature relies on using simplified kinetic models to interpret measurements of cellulose weight loss during heating.^{12–16} Experimental data are then fitted to a given model to extract kinetic parameters such as the apparent activation energy, which represents an average over the barriers of the underlying microscopic processes. Apparent activation energies may also include contributions from phase changes, e.g., vaporization of

volatile pyrolysis products, rendering such apparent activation energies as mixtures of intrinsic kinetics and thermodynamic quantities. Reported activation energies cover a rather wide range, from 13 to 67 kcal/mol,⁹ likely because of the strongly differing assumptions invoked by the various models. A small subset of this diverse collection of empirical models has fitted pre-exponential factors falling in the range of 10¹³–10¹⁴ s^{–1}, typical of vibrational attempt frequencies.⁹ The apparent activation energies from this subset lie in a much narrower range: 45.4–47.8 kcal/mol.^{9,17–21} Below we report on a microscopic unimolecular process that accounts for the major pyrolysis product and whose barrier fits into this experimental “energy budget”.

One of the most widely used models is the Broido-Shafizadeh model,^{18,22,23} which assumes that cellulose first converts to “active cellulose” and then further degrades via parallel pathways either to volatile organic compounds or to char and gases (CO, CO₂, H₂O). Many variations to this model exist in the literature;^{9,17,19–21,24–31} several of these omit the active cellulose step and assume that cellulose pyrolyzes directly to volatiles, char, and gases.^{20,29,32,33} Recently, Lin et al.⁹ suggested that the phase change to active cellulose is a

Received: May 26, 2012

Published: August 13, 2012

reversible transformation observed below 260 °C, while others have suggested that active cellulose is a liquid material formed irreversibly above 260 °C due to cellulose depolymerization.^{18,34–36}

The detailed product distribution from cellulose pyrolysis also varies considerably with reaction conditions. Although there is broad agreement that the major product of cellulose fast pyrolysis (400–600 °C) is the anhydrosugar levoglucosan (LGA),⁹ it is not clear how LGA forms or why it is the major product. Mettler et al. recently showed that the fraction of LGA produced depends strongly on whether cellulose pyrolysis takes place in powder or thin-film samples,³⁷ suggesting a kinetically controlled product distribution. In addition, the formation mechanisms of furans and fragmentation products such as formic acid, which are observed in appreciable quantities, remain under debate. In particular, while some researchers believe these products form from anyhydrosugars,^{9,38} others believe they arise directly from cellulose via parallel pathways.^{17,25,39,40} This level of uncertainty underscores the need for microscopic approaches to reveal atomic-level details of cellulose decomposition chemistry.

We recently reported a classical molecular dynamics study of the thermophysical properties of cellulose I β upon heating up to 250 °C.⁸ We found that above 175 °C the cellulose I β solid undergoes substantial thermal expansion, and the hydrogen-bonding pattern changes from primarily intrachain to mostly interchain hydrogen bonding. Formation of these interchain hydrogen bonds upon heating and their stabilizing effect on the cellulose solid matrix explain why cellulose does not undergo the typical physical phase change to a melt. This suggests that thermal depolymerization is necessary to explain the observation of a liquid intermediate during cellulose pyrolysis.^{18,34–36} Because of possible confusion about the oft-used term active cellulose, we define “reversible active cellulose” below 260 °C as the expanded but chemically intact form of cellulose dominated by interchain hydrogen bonding⁸ and distinguish this from “liquid intermediate cellulose” above 260 °C, which is likely the product of depolymerization reactions. The present work is focused on discovering the nascent reactive events that depolymerize cellulose chains, representing the first chemical steps toward forming liquid intermediate cellulose. We are particularly interested in revealing the depolymerization pathways that lead to precursors of major pyrolysis products such as LGA. We also wish to determine whether the thermal expansion and interchain hydrogen bonding, present in reversible active cellulose, are important for promoting the chemistry that leads to liquid intermediate cellulose and pyrolysis products.

Modeling a complex process like pyrolysis is a daunting computational task due to the hundreds of products formed and the paucity of molecular information on intermediate species. Because of this, most efforts in this direction are based on using simple models of cellulose such as glycerol,^{41,42} 2,3,4-hydroxyl-butyraldehyde,⁴³ 2,3,4-hydroxyl-butyric acid,⁴³ methyl-glucoside,⁴⁴ glucose,^{45,46} levoglucosan (LGA),^{47,48} cellobiose,^{49,50} methyl-cellobiose,⁵¹ and cellotriose.⁵² For example, Geng et al.⁴¹ and Nimlos et al.⁴² performed quantum calculations to compute the pyrolytic pathways of gas-phase glycerol, considering it as a model for sugars since glycerol has three adjacent hydroxyl groups and is small enough to be modeled with high-level quantum calculations. They explained formation of acetaldehyde, which is the major product of glycerol pyrolysis. Hosoya et al. studied formation of LGA

using methyl-glucoside as model for cellulose.⁴⁴ They considered homolytic, heterolytic, and concerted mechanisms to form LGA and found that the concerted mechanism is the kinetically most favorable pathway to form LGA. Very recently, Mayes and Broadbelt reported DFT calculations on methyl-cellobiose with a continuum treatment of the cellulose environment,⁵¹ finding a mechanism of LGA generation in good agreement with the concerted pathway reported by Hosoya et al. Assary and Curtiss performed DFT calculations showing that cellobiose first depolymerizes to produce 1,2-dehydroglucopyranose, which further converts to LGA via 1,6-epoxide formation.⁵⁰ In general, these gas-phase computational studies provide putative mechanisms that may underlie cellulose pyrolysis. However, solid-state packing and intra/interchain hydrogen bonding⁸ may strongly influence decomposition pathways and energetics. To address this, we performed reaction dynamics calculations in the solid state to simulate thermal decomposition of cellulose I β using two unit cells of cellulose I β under three-dimensional periodic boundary conditions.

Investigating cellulose pyrolysis mechanisms without bias toward previously determined gas-phase pathways relies on a computational method for harvesting reactive events at the target temperature regime. Reactive molecular dynamics (MD) can furnish such an approach provided there is sufficient accuracy in the chemical forces of bond breaking and making, and there is efficient sampling of rare reactive events.⁵³ Various reactive MD approaches include MD using reactive force fields,^{54,55} reactive MD based on switching functions,⁵⁶ and ab initio MD (AIMD) simulations.^{11,57} In general, reactive force fields provide less computationally expensive force calculations and hence can be run for longer physical times compared to ab initio methods. However, much accuracy can be lost by reactive force fields, especially when such force fields have been fitted to account for only a specific kind of process. Cellulose pyrolysis may involve homolytic scission, heterolytic bond breaking, charge transfer, and stabilization by anchimeric assistance and/or hydrogen bonding. Instead of attempting to build all these effects into a reactive force field, we turned to ab initio Car–Parrinello MD (CPMD) simulations, in which valence electrons and ions (nuclei plus core electrons) are propagated together in an extended-Lagrangian formulation of Born–Oppenheimer classical mechanics.¹¹

Mettler et al. recently showed through thin-film experiments that cyclohexaamylose can be used as a surrogate for cellulose.³⁷ Such thin-film studies provide a reliable window into isothermal kinetics of cellulose pyrolysis. Mettler et al. also performed CPMD simulations on solid cyclohexaamylose in a periodic box of dimensions 14 Å \times 14 Å \times 9 Å based on the 13.5 Å external diameter of cyclohexaamylose.^{58,59} To accelerate the dynamics, Mettler et al. performed their CPMD simulations at much higher temperatures (1700–1900 °C) than the temperature used in their thin-film pyrolysis experiments (500 °C). These CPMD simulations predict that hydroxy-methylfurfural (HMF), glycoaldehyde, formic acid, and carbon monoxide are formed through an initial *homolytic* cleavage of the glycosidic bond. Despite this progress, it remains unclear whether homolytic C–O cleavage persists as the dominant depolymerization mechanism at the much lower temperatures of fast pyrolysis (400–600 °C). In the present work, we address this issue by focusing on experimental conditions and applying specialized computational techniques for efficient sampling of rare events.

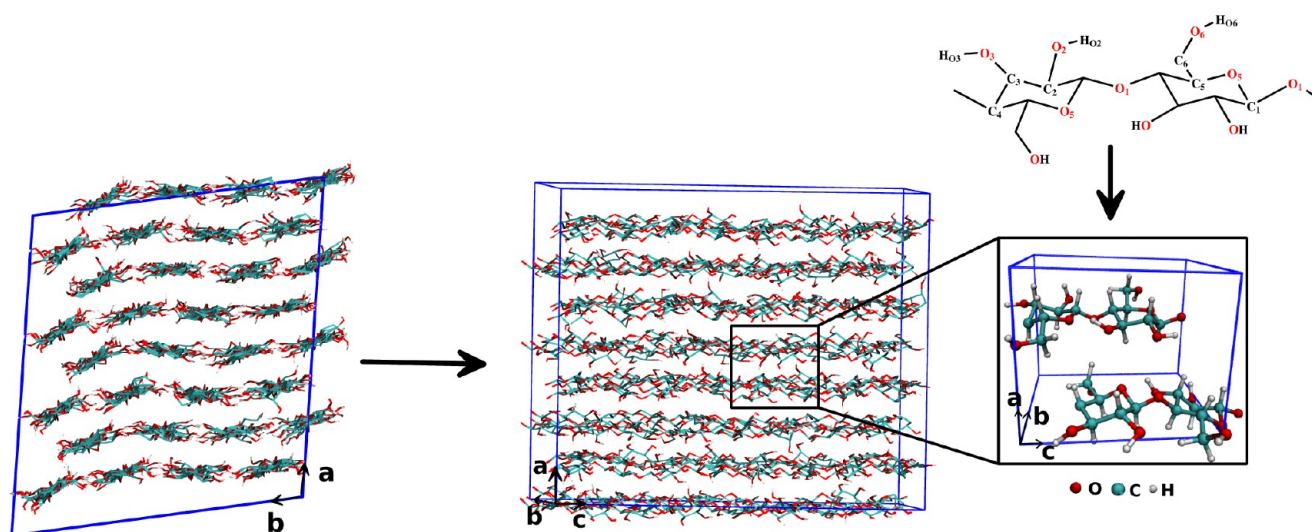


Figure 1. Simulation cell of cellulose *I* β containing 2 cellobiose units at 327 °C extracted from an equilibrated system of 128 cellobiose units. Standard atom numbering in the literature is shown on top. For clarity, hydrogens on carbon atoms are not shown in the 2D representation.

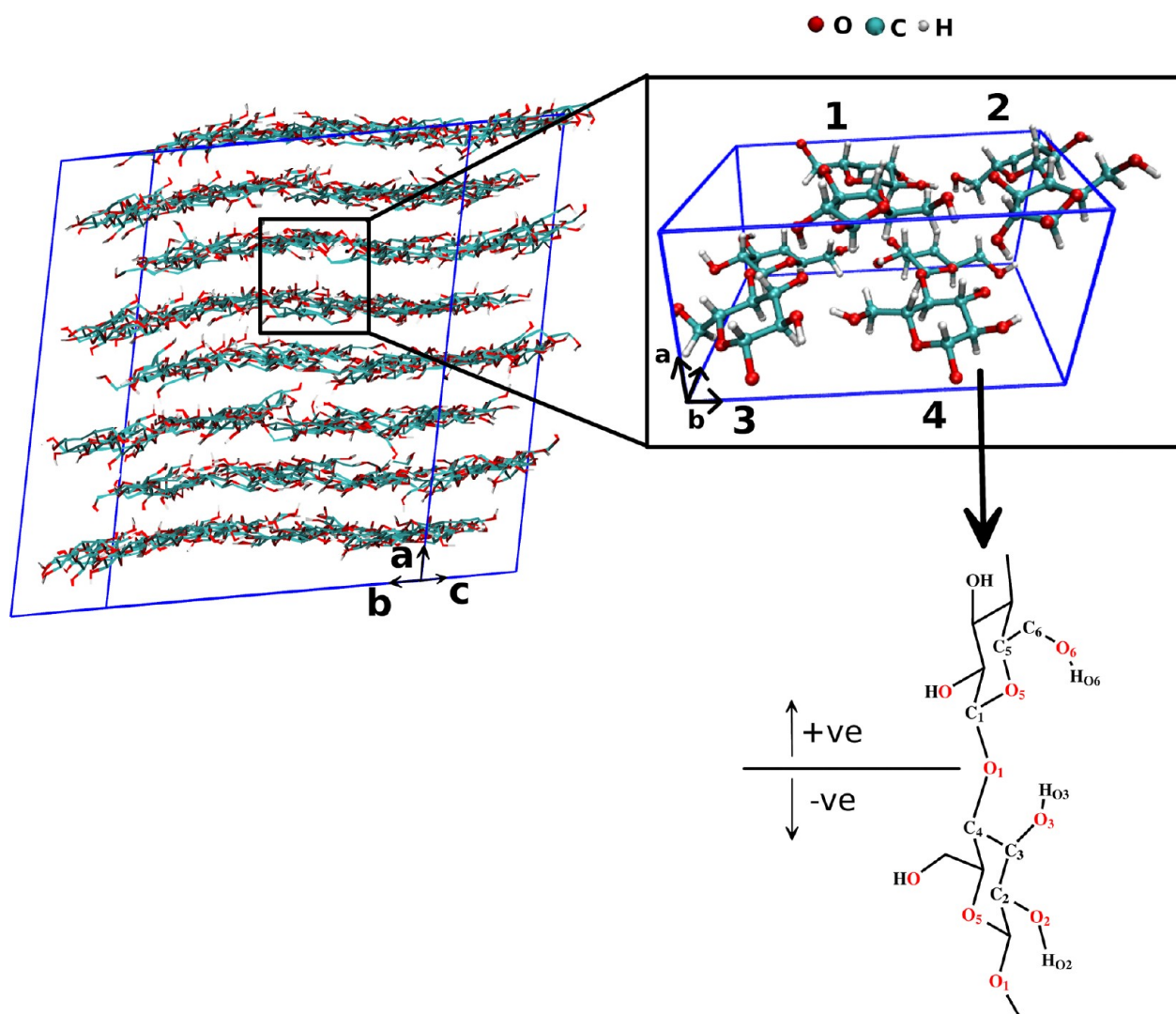


Figure 2. Simulation cell of cellulose *I* β containing 4 cellobiose units at 327 °C. Cellobiose chains are numbered as 1, 2, 3, and 4. For clarity, hydrogens on carbon atoms are not shown in the 2D representation of cellobiose chains.

Molecular dynamics is generally plagued by the need to use very short time steps—usually around 1 fs in classical simulations and even shorter time steps in AIMD—to guarantee dynamical stability. As a consequence, classical MD is usually restricted to 10–100 ns time scales, while the great computational expense of AIMD restricts it to 10–100 ps in physical duration. To put this time scale into perspective, we consider a $\tau = 100$ ps Arrhenius process occurring at 600 °C ($T = 873$ K) with an attempt frequency of $\nu = 10^{13}$ s⁻¹. This corresponds to an activation energy of $E_{\text{act}} = RT \ln(\nu\tau) = (1.75 \text{ kcal/mol}) \times \ln(1000) = 12 \text{ kcal/mol}$. For comparison, apparent activation energies extracted from cellulose pyrolysis experiments (reporting pre-exponentials in the range 10^{13} – 10^{14} s⁻¹) fall in the range of 45–48 kcal/mol,^{9,17–21} corresponding to a time scale of about 0.1 s, well outside the MD window.

Accelerated MD methods that address this time scale problem include parallel-replica dynamics,⁶⁰ hyperdynamics,^{61,62} temperature-accelerated dynamics,⁶³ and metadynamics,⁶⁴ each with its unique set of advantages. The acceleration in parallel-replica dynamics is limited to the number of parallel MD simulations that can be performed and hence is computationally limited in AIMD. The acceleration in hyperdynamics often strays to ancillary, low-frequency modes in molecular solids.⁶⁵ Temperature-accelerated dynamics requires performing simulations at much higher temperatures, which may activate different and irrelevant mechanisms. Metadynamics requires specifying certain collective variables on which to focus the dynamical acceleration. At first blush it may seem that one needs to know the mechanism a priori to effectively apply metadynamics. However, reaction mechanisms can be explored and harvested with this method by identifying vibrational motions that likely encompass reaction coordinates key to cellulose pyrolysis. Below we report our application of CPMD-metadynamics to this problem, finding that collective variables involving glycosidic C–O bonds and nearby polar hydrogens open up a vast array of depolymerization processes. Moreover, the metadynamics method allows estimates of free energy barriers, facilitating comparison with experimental activation energies. Below we find that cellulose expansion and hydrogen bonding are indeed key for the predicted depolymerization pathways. We also find at 600 °C that depolymerization to a precursor of LGA is the kinetically favored mechanism, suggesting why LGA is the major product under fast pyrolysis conditions.

The remainder of this article is organized as follows: in section 2 we briefly describe the methods used to generate initial cellulose densities and structures at high temperatures; we also offer computational details regarding the CPMD-metadynamics simulations. In section 3, we give results and discussion of the nascent decomposition pathways at 327 and 600 °C. Finally, in section 4, we offer concluding remarks. We also provide extensive computational details of the methods used in this work, thermochemistry of representative cellulose pyrolysis reactions, changes in distance of selected atoms during CPMD-metadynamics run, and infrared (IR) spectra of the key intermediate in the Supporting Information, along with movies of selected CPMD-metadynamics runs.

2. METHODS AND COMPUTATIONAL DETAILS

Here we provide a brief description of the methods used in this work. A detailed description of the computational approach can be found in the Supporting Information.

2.1. Simulation Cell. We performed classical NPT MD simulations performed on $4 \times 4 \times 4$ units of cellulose I β (5888 atoms) at 1 atm pressure and temperatures of 327 and 600 °C to generate equilibrated structures using the GROMACS 4.07 simulation package.^{66,67} GROMOS-45a4, a united (CH and CH₂) atom force field developed for hexapyranose-based carbohydrates,⁶⁸ was used for this part of the study. This resulted in three simulation cells studied below:

- 1unit, one unit cell of cellulose I β with density appropriate for 327 °C (see Figure 1);
- 2unitD, two unit cells of cellulose I β (repetition along the *b* axis) with density appropriate for 327 °C (see Figure 2);
- 2unitE, two unit cells of cellulose I β with density appropriate for 600 °C (see Figure 3).

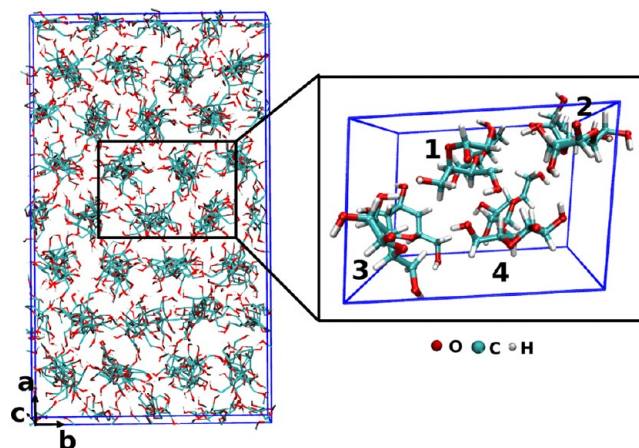


Figure 3. Simulation cell of cellulose I β containing 4 cellobiose units at 600 °C. Each atom in the simulation cell is numbered as before. For clarity, hydrogens on carbon atoms are not shown in the 2D representation of cellobiose chains.

Below we study 2unitD at 327 °C, 2unitD at 600 °C, and 2unitE at 600 °C to disentangle the effects of density and temperature on cellulose pyrolysis. The equilibrated structures at 327 and 600 °C, along with the extracted simulation cells and the numbering scheme used in this work, are shown in Figures 2 and 3, respectively.

2.2. Ab Initio Calculations. Ab initio MD simulations based on the Car–Parrinello scheme¹¹ have been performed in this work within the Kohn–Sham formulation of density functional theory (DFT)^{69,70} using the CPMD software package 3.15.1.⁷¹ The DFT electronic energy was computed with the Becke–Lee–Yang–Parr (BLYP)^{72,73} gradient-corrected exchange–correlation functional; below we analyze the accuracy of this approach through detailed comparisons with appropriate all-electron quantum calculations. A planewave basis set⁷⁴ was used to expand the Kohn–Sham orbitals. Chemically inactive core electrons were represented by norm conserving Goedecker–Teter–Hutter pseudopotentials.⁷⁵ This functional/pseudopotential has previously been shown to give good performance for glucopyranose systems.^{76–78}

To determine an optimal planewave cutoff, we performed both CPMD and all-electron calculations using Gaussian09⁷⁹ on the gas-phase reaction of cellobiose yielding glucose and levoglucosan (see Supporting Information, Figure S1, Reaction 1). Details of these calculations are summarized in the Supporting Information. As shown in Supporting Information Figure S3, we found that a cutoff of 70 Ry is sufficient to converge this reaction energy. A cutoff of 70 Ry for the Goedecker pseudopotential was also shown to be sufficient for the glucopyranose system.^{76–78} We found, in particular, that the CPMD reaction energy computed as described above is essentially identical to that obtained by all-electron DFT methods at the BLYP/cc-pvqz(opt)//BLYP/aug-cc-pvqz(sp) model chemistry (i.e., single-

Table 1. Comparison of All Electronic Structure Calculations with CPMD Simulations

	Reaction scheme	Temperature	Energy Barriers (kcal/mol)								$\left \frac{\Delta G_{\text{BLYP}}^{\ddagger} - \Delta G_{\text{CPMD}}^{\ddagger}}{\Delta G_{\text{CPMD}}^{\ddagger}} \right a$	$\left \frac{\Delta G_{\text{MP2}}^{\ddagger} - \Delta G_{\text{BLYP}}^{\ddagger}}{\Delta G_{\text{MP2}}^{\ddagger}} \right b$
			CPMD/BLYP		BLYP				MP2			
			ΔF^{\ddagger} (50Ry)	ΔF^{\ddagger} (70Ry)	6-311G(d,p)	ΔE^{\ddagger}	ΔG^{\ddagger}	cc-pvqz ^c	ΔE^{\ddagger}	ΔG^{\ddagger}		
methyl -glucoside		327 °C	59	49	47	44	49	46	71	68	0.07	0.35
cellobiose		327 °C	51	43	55	46	54	45	81	72	0.04	0.36
cellobiose		600 °C	—	—	55	44	54	42	81	70	—	0.37

^aBLYP/cc-pvqz compared with CPMD/70 Ry. ^bBLYP and MP2 both at 6-311G(d,p). ^cOnly single-point energy calculations were performed using the optimized geometry of BLYP/6-311G(d,p); zero-point, thermal, enthalpic, and entropic corrections were computed using BLYP/6-311G(d,p).

point energy correction using BLYP/aug-cc-pvqz^{80–82} on optimized geometries obtained with BLYP/cc-pvqz^{80,81}).

We repeated this reaction energy comparison for 11 more reactions representative of cellulose decomposition, considering the following reactants: cellobiose, glucose, levoglucosan, levoglucosenone, 1,4:3,6-dianhydro- β -D-glucopyranose (DGP), hydroxy-methylfurfural (HMF), furfural, glycoaldehyde, water, and several precursors that result from the CPMD studies detailed below (see Supporting Information for a complete list of reactions). In all these cases, we found that CPMD reaction energies using BLYP/Goedecker/70 Ry are very close to all-electron results using BLYP/cc-pvqz(opt)//BLYP/aug-cc-pvqz(sp). However, for a simulation cell equivalent to two unit cells of cellulose I β (periodically repeated to mimic the cellulose matrix) consisting of 516 valence electrons, the cutoff of 70 Ry is computationally too expensive for CPMD production runs of cellulose decomposition. Therefore, in order to make these simulations computationally tractable, a lower cutoff of 50 Ry was used for computing free-energy barriers of processes in cellulose decomposition. The effect of using a lower cutoff is analyzed and discussed in detail in section 3. As shown below, we find that using a cutoff of 50 Ry overestimates the barrier of a representative test reaction by 10 kcal/mol, or about 20% of the barrier height.

The metadynamics method designed by Parrinello and co-workers^{64,83–85} was used to explore cellulose pyrolysis chemistry. Although metadynamics produces rigorously incorrect dynamics, the trajectories can be used to harvest free-energy barriers for rare events. Metadynamics requires specification of collective variables defining the essential modes associated with the desired transitions in the simulated system. The design of collective variables to explore the cellulose pyrolytic pathways is described below. The remaining parameters required by the CPMD-metadynamics simulations are provided in the Supporting Information (see section S1).

To investigate possible spectroscopic signatures of reactive intermediates in cellulose pyrolysis, we computed IR spectra of constrained gas-phase cellobiose and pre-LGA using Gaussian09 with B3LYP/6-311G(g,p). Vibrational frequencies were scaled⁸⁶ with the factor 0.9769. Configurations were generated from equilibrated solid cellulose (and depolymerized solid cellulose) at 600 °C as discussed in section 2.5.

2.3. Nomenclature. Due to the relatively large number of atoms in the CPMD simulation cell, we adopted the following nomenclature to distinguish each atom for specifying CVs. Since cellulose is a

homopolymer of glucose residues connected by β -(1–4) glycosidic linkages, each atom in a glucose residue was distinguished by the standard numbering adopted in the literature for glucose.⁸ Each glucose residue was distinguished with respect to the middle O₁ oxygen as shown in Figure 2 (away from the reader as *positive* and toward the reader as *negative*). A number was assigned to each cellulose chain also shown in Figure 2. For example, C₁ toward the reader from the middle O₁ atom on the cellulose chain numbered 2 is denoted as ²-C₁ atom, where the superscript “2–” means chain 2 and toward the reader, using Figure 2 as reference. The middle glycosidic oxygen O₁ on chain 3 is labeled as “³O₁.”

2.4. Collective Variables. In this work we used two different types of collective variables for performing metadynamics simulations. The first one is the distance between two atoms, A and B, and the second is the coordination number of a selected atom A with respect to *k* number of selected atoms B. The functional form of these collective variables is detailed in the Supporting Information (see section S1.4).

In principle, all unknown pyrolysis pathways can be generated by running CPMD-metadynamics using a sufficiently diverse library of CVs. In practice, due to the limitation of computational resources, we constrained our exploratory search to a targeted subset of CVs. These were inspired from our focus on investigating depolymerization and ring-opening reactions. The resulting list of CVs used in this work is described below. In general, we found that considering 2 CVs in each CPMD-metadynamics run was sufficient.

- The coordination number of a glycosidic oxygen (O₁) with respect to bonded carbon atoms (⁺C₁ and [–]C₄), and the coordination number of O₁ with respect to neighboring polar hydrogens. Several combinations of coordination numbers of O₁ with respect to only a single neighboring polar hydrogen were also studied.
- The coordination number of a ring oxygen (O₅) with respect to bonded carbon atoms (C₁ and C₅), and the coordination number of O₅ with respect to neighboring polar hydrogens.
- The coordination number of O₁ with respect to bonded carbon atoms (⁺C₁ and [–]C₄), and the coordination number of O₆ with respect to either or both C₁ and C₂.
- The coordination number of O₆ with respect to C₁, and the coordination number of O₁ with respect to the hydrogen bonded to O₆ (i.e., H_{O6}).

Table 2. Nascent Processes Occurring during Pyrolysis^a

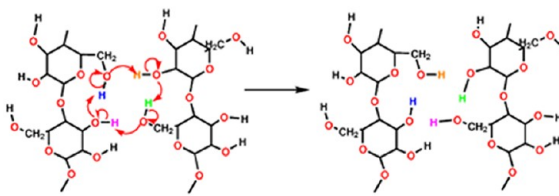
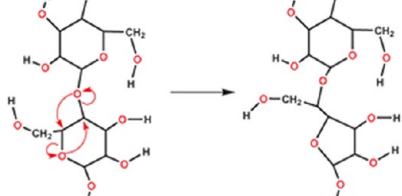
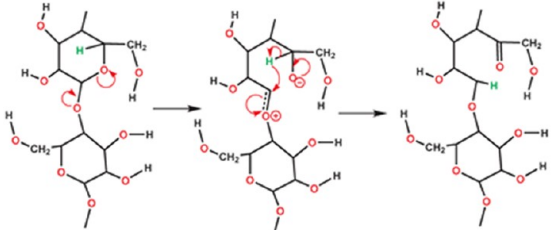
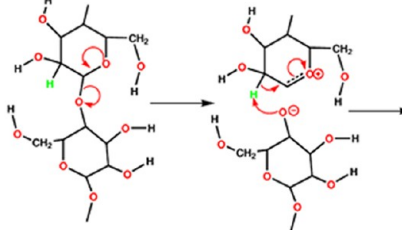
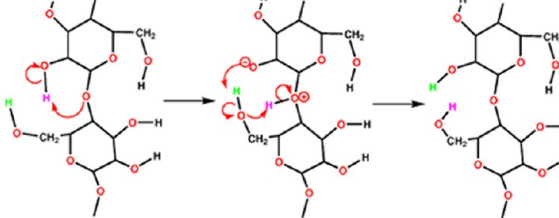
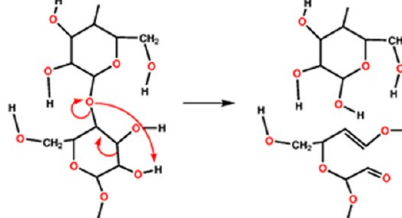
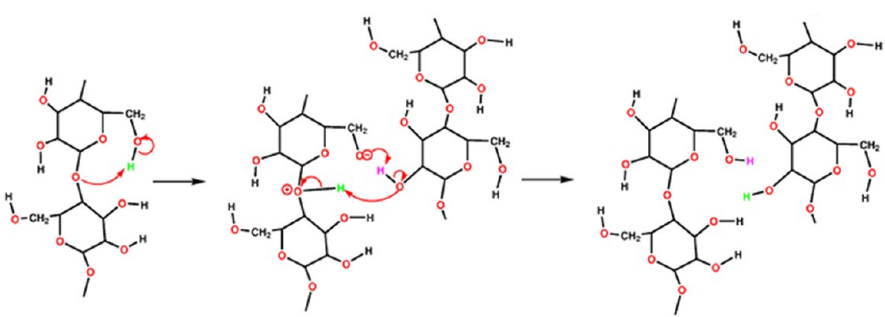
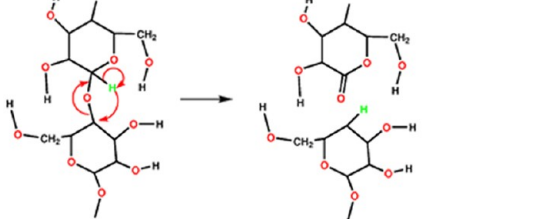
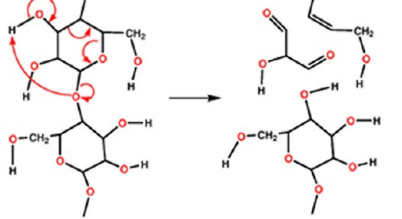
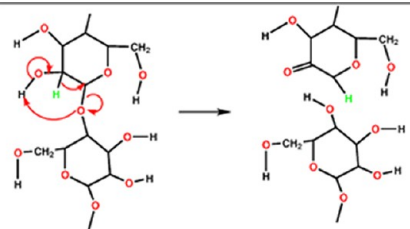
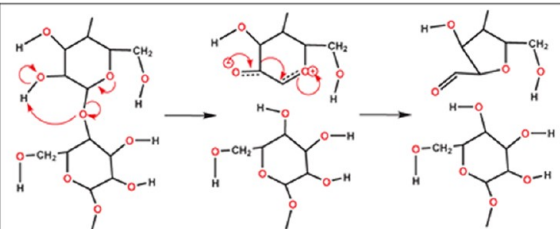
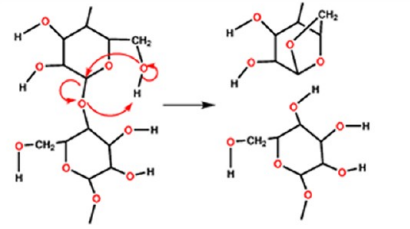
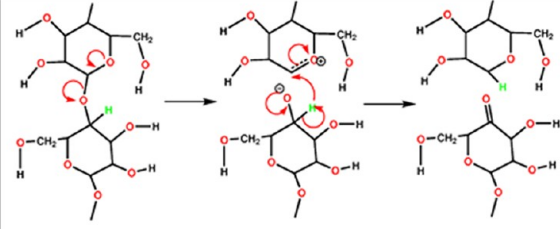
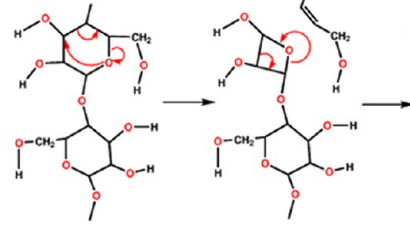
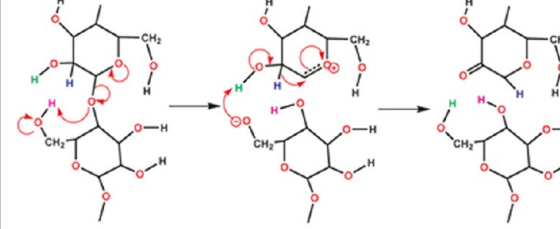
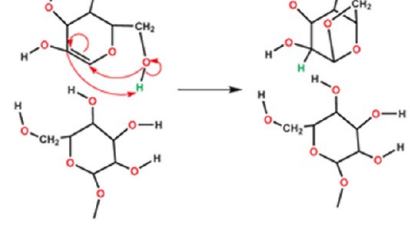
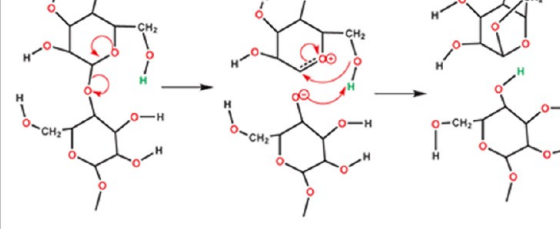
(A)		(B)	
Rearrangement of hydrogens		Ring contraction	
(C)		(D)	
De-polymerization, Ring opening		De-polymerization, Elimination	
(E)		(F)	
Hydrogen rearrangement		De-polymerization, Ring opening	
(G)			
Hydrogen rearrangement			
(H)			
De-polymerization			
(I)			
De-polymerization, Ring fragmentation			

Table 2. continued

<p>(J)</p>  <p>De-polymerization</p>	<p>(K)</p>  <p>De-polymerization, Ring contraction, precursor to HMF</p>
<p>(L)</p>  <p>De-polymerization, 1,6 epoxide formation, precursor to LGA</p>	<p>(M)</p>  <p>De-polymerization</p>
<p>(N)</p>  <p>De-polymerization, Ring fragmentation, evolution of formic acid</p>	<p>(O)</p>  <p>De-polymerization</p>
<p>(P)</p>  <p>1,6 epoxide formation, precursor to LGA</p>	<p>(Q)</p>  <p>De-polymerization, 1,6 epoxide formation, precursor to LGA</p>

^aFor clarity neighboring cellulose chains have been removed in the following representation.

2.5. Benchmarking Barriers. We performed several gas-phase calculations to benchmark the errors in the free-energy barriers computed using CPMD-metadynamics on solid cellulose. These gas-phase calculations were performed with both CPMD-metadynamics and Gaussian09 on both unconstrained (Table 1, row 1) and

constrained systems (Table 1, rows 2 and 3). The unconstrained system we studied is gas-phase methyl- β -D-glucoside reacting to form LGA and methanol, allowing comparison with the previous calculations of Hosoya et al.⁴⁴ The constrained system we studied is cellobiose glycosidic elimination, allowing comparison with our solid

Table 3. Collective Variables, Reactions Observed, and Estimate of Free-Energy Barriers

CV set no.	Collective Variable	Atom Labels		Reaction Scheme ^a			Free-Energy Barrier (kcal/mol)		
		Var1	Var2	327 °C (D)	600 °C (D)	600 °C (E)	327 °C (D)	600 °C (D)	600 °C (E)
1	c(O–C)	⁴ O ₁	⁴⁺ C ₁ , ^{4–} C ₄	A	spu	D	28	—	42
	d(O–H)	⁴⁺ O ₆	⁴⁺ H _{O6}						
2	c(O–C)	⁴ O ₁	⁴⁺ C ₁ , ^{4–} C ₄	B	H	M	48	38	34
	c(O–H)	⁴ O ₁	^{4–} H _{O6}						
3	c(O–C)	⁴ O ₁	⁴⁺ C ₁ , ^{4–} C ₄	E	J	K	55	59	49
	c(O–H)	⁴ O ₁	⁴⁺ H _{O2}						
4	c(O–C)	⁴ O ₁	⁴⁺ C ₁ , ^{4–} C ₄	D	spu	M	42	—	36
	c(O–H)	⁴ O ₁	^{4–} H _{O3}						
5	c(O–C)	⁴ O ₁	⁴⁺ C ₁ , ^{4–} C ₄	B	spu	—	25	—	—
	c(O–H)	⁴ O ₁	⁴⁺ H _{C2}						
6	c(O–C)	⁴⁺ O ₆	⁴⁺ C ₁	G	E	L	—	42	126
	c(O–H)	⁴ O ₁	⁴⁺ H _{O6}						
7	c(O–C)	⁴⁺ O ₅	⁴⁺ C ₁ , ⁴⁺ C ₅	C	B ^b	—	35	22	—
	c(O–H)	⁴⁺ O ₅	^{4–} H _{O3} , ⁴⁺ H _{O6} , ²⁺ H _{O6}						
8	c(O–C)	⁴ O ₁	⁴⁺ C ₁ , ^{4–} C ₄	B	O	—	34	43	—
	c(O–H)	⁴ O ₁	⁴⁺ H _{O2} , ⁴⁺ H _{O6} , ^{4–} H _{O3} , ^{4–} H _{O6} , ¹⁺ H _{O2} , ^{1–} H _{O6}						
9	c(O–C)	⁴ O ₁	⁴⁺ C ₁ , ^{4–} C ₄	B	—	—	20	—	—
	c(O–H)	⁴ O ₁	⁴⁺ H _{O2} , ⁴⁺ H _{O6} , ^{4–} H _{O3} , ^{4–} H _{O6} , ¹⁺ H _{O2} , ^{1–} H _{O6} , ^{4–} H _{C6a} , ^{4–} H _{C6b} , ^{1–} H _{C6a} , ^{1–} H _{C6b}						
10	c(O–C)	⁴ O ₁	⁴⁺ C ₁ , ^{4–} C ₄	—	—	F	—	—	50
	c(O–H)	⁴ O ₁	⁴⁺ H _{O6} , ^{4–} H _{O2} , ⁴⁺ H _{O2} , ¹⁺ H _{O6} , ^{4–} H _{O6} , ³⁺ H _{O6} , ^{3–} H _{O6}						
11	c(O–C)	⁴ O ₁	⁴⁺ C ₁ , ^{4–} C ₄	—	—	H	—	—	35
	d(O–C)	⁴⁺ O ₆	⁴⁺ C ₁						
12	c(O–C)	⁴ O ₁	⁴⁺ C ₁	spu	M	I	—	31	33
	d(O–C)	⁴⁺ O ₆	⁴⁺ C ₁						
13	c(O–C)	⁴ O ₁	⁴⁺ C ₁	—	—	D	—	—	43
	d(O–C)	⁴ O ₁	⁴⁺ H _{O6}						
14	c(O–C)	⁴⁺ O ₆	⁴⁺ C ₁	—	—	L	—	—	69
	c(O–H)	⁴ O ₁	⁴⁺ H _{O6} , ^{4–} H _{O2} , ⁴⁺ H _{O2} , ¹⁺ H _{O6} , ^{4–} H _{O6} , ³⁺ H _{O6} , ^{3–} H _{O6}						
15	c(O–C)	⁴⁺ O ₆	⁴⁺ C ₁	—	—	D	—	—	40
	c(O–H)	⁴ O ₁	^{4–} H _{O2}						
16	c(O–C)	⁴⁺ O ₅	⁴⁺ C ₁ , ⁴⁺ C ₅	—	—	N	—	—	61
	c(O–H)	⁴⁺ O ₅	^{4–} H _{O2} , ¹⁺ H _{O6} , ³⁺ H _{O2}						
17	c(O–C)	⁴ O ₁	⁴⁺ C ₁	c	D	Q	69	37	36
	c(O–C)	⁴⁺ O ₆	⁴⁺ C ₂						
18 ^d	c(O–C)	⁴⁺ O ₆	⁴⁺ C ₁ , ⁴⁺ C ₂	—	—	P	—	—	89
	c(H–C)	⁴⁺ H _{O6}	⁴⁺ C ₁ , ⁴⁺ C ₂						

^a“spu” refers to spurious reaction mechanism observed due to limitation of the size of simulation cell. ^bRing contraction takes place in the opposite ring in comparison to shown in Table 2 ^cWe observed formation of precursor to LGA via interchain exchange of hydrogen. ⁴⁺H_{O6} is transferred to ^{1–}O₆, which in turn transfers ^{1–}H_{O6} to ⁴O₁ when ⁴⁺O₆ completes a bond with ⁴⁺C₁. ^dThe reactants are products of reaction scheme D.

cellulose results. By comparing gas-phase and solid CPMD-metadynamics results, we also reveal solid-state effects on mechanisms and barriers in cellulose pyrolysis. All barriers were confirmed with normal-mode analysis and steepest-descent relaxations. Gaussian09 barriers were computed with BLYP and MP2 to quantify DFT errors. More details on these barrier calculations can be found in the Supporting Information.

For the constrained study of gas-phase cellobiose reactivity, we began by running CPMD-metadynamics on *solid* cellulose at 327 °C in the 2unitD cell using CV set 4 in Tables 2 and 3. Gas-phase Gaussian09 and CPMD-metadynamics calculations were then performed to analyze/interpret the solid cellulose results. The inputs for these gas-phase (and IR spectra) calculations were obtained as follows.

- Transition-state searches were initiated from the 2unitD solid cellulose configuration at the transition state of free energy.
- All chains were deleted from the simulation cell except for the chain where the reaction takes place.
- One end of this chain was terminated with a hydrogen atom and the other with an OH group to complete the cellobiose unit (the coordinates of the oxygen atom were obtained from the periodic image of the simulation cell).
- Oxygen atoms were clamped on both ends to mimic the packing of a cellulose polymer.

3. RESULTS AND DISCUSSION

We begin by presenting CPMD and Gaussian calculations on the conversion of methyl- β -D-glucoside to levoglucosan (LGA)

in the gas phase to benchmark the accuracy and performance of the CPMD-metadynamics approach. We then present cellulose calculations establishing the system size effects at 327 °C, which is followed by calculations of cellulose decomposition at 327 and 600 °C at various densities to determine how reaction pathways vary with density and temperature. Finally, we summarize our work by comparing with previous calculations and experimental results.

3.1. Benchmark I: Gas-Phase Methyl- β -D-glucoside to LGA. To benchmark the CPMD-metadynamics calculations of free-energy barriers, we first performed CPMD-metadynamics calculations studying conversion of isolated gas-phase methyl- β -D-glucoside to LGA and methanol at 327 °C for comparison with the reaction mechanism previously computed by Hosoya et al.⁴⁴ A detailed picture of methyl- β -D-glucoside along with its numbering scheme is shown in Figure 4. We used the distance between O₆–H_{O6} [$d(\text{O}_6\text{--H}_{\text{O6}})$] and C₁–O₁ [$d(\text{C}_1\text{--O}_1)$] as the set of CVs for these calculations.

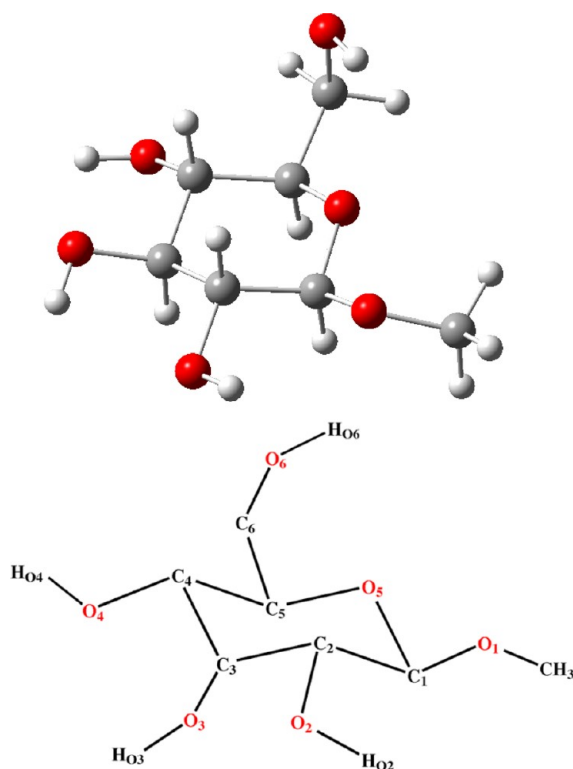


Figure 4. Numbering scheme used for methyl β -D-glucoside in a $^1\text{C}_4$ chair conformation. For clarity, hydrogens on carbon atoms are not shown in the 2D representation.

At ~ 45 ps, we found the methyl- β -D-glucoside converts to LGA through a concerted mechanism via O₆ nucleophilic attack on the “anomeric” C₁, releasing methanol. Like Hosoya et al.⁴⁴ we found a concerted mechanism to form LGA. The first step proposed by Hosoya et al.⁴⁴ is a conformational change from the $^1\text{C}_4$ chair (shown in Figure 4) to the $^4\text{C}_1$ chair conformation. Due to the type of collective variables used in our CPMD-metadynamics run, this conformational change was not resolved in the resulting free-energy surface. However, by analyzing the C₁–O₅–C₅–C₄ ring dihedral angle during the simulation we found a jump (data not shown) from $+40^\circ$ to -40° by metadynamics step 9000, indicating that indeed a conformational change is predicted prior to nucleophilic attack.

A movie of the CPMD-metadynamics run is provided in the Supporting Information. We note that the movie software draws strong hydrogen bonds (shorter than 1.7 Å) as normal bonds, which may suggest multivalent hydrogens.

To further investigate the mechanism of this process, we took the CPMD-metadynamics configuration at the transition state of free energy as an initial condition for a transition state search in Gaussian09 using BLYP/6-311G(d,p) as the model chemistry. The conformational change was again observed as the first step in the overall process when the transition state obtained by BLYP/6-311G(d,p) was relaxed along the reaction coordinate toward the reactant state.

With a CPMD planewave cutoff of 70 Ry, we found a free-energy barrier for this process of 50 kcal/mol. To check the repeatability of this result, we performed CPMD-metadynamics using velocities and coordinates obtained by equilibrating the input from the above run for another 6 ps. We found the same reaction mechanism and a free-energy barrier from this second run of 51 kcal/mol, indicating good repeatability, well within the 2.5 kcal/mol Gaussian height used for the bias potential, which serves as a natural error bar for the metadynamics method. Below we report simulations on solid cellulose using the lower planewave cutoff of 50 Ry. To investigate the effect of a lower cutoff, we revisited CPMD-metadynamics of methyl- β -D-glucoside with a cutoff of 50 Ry. We found the same mechanism for formation of LGA; however, we found that the free-energy barrier is overestimated by 10 kcal/mol ($\sim 20\%$) with the 50 Ry cutoff. We take this error into account below when comparing with experimental data on cellulose pyrolysis.

We now use this gas-phase system to analyze the accuracy of the CPMD-metadynamics free-energy barriers. Row 1 in Table 1 summarizes the results from Gaussian09 calculations of the Gibbs free energy for this reaction at BLYP/6-311G(d,p) and with single-point corrections to the barrier using BLYP/cc-pvqz and MP2/6-311G(d,p). We found a free-energy barrier of 44 kcal/mol using BLYP/6-311G(d,p), already indicating fairly good agreement with CPMD-metadynamics, but outside the 2.5 kcal/mol error bar of this approach. The free energy with single-point correction at BLYP/cc-pvqz was found to be 46 kcal/mol, which is 8% less than that obtained from the CPMD-metadynamics run using a cutoff of 70 Ry. This agreement is consistent with our computed thermochemistry data, showing that a cutoff of 70 Ry gives results comparable to BLYP/cc-pvqz for several representative cellulose pyrolysis reactions (see Supporting Information). The free energy with single-point correction at MP2/6-311G(d,p) was found to be 68 kcal/mol, which is 35% higher than that found with BLYP/6-311G(d,p), a result qualitatively consistent with our previous proton transfer calculations.⁸⁷ MP2 corrections to other barriers studied below are also around 36–37%, a result we utilize below when comparing our cellulose decomposition results with experiments. Below we compare our present results with the barriers computed by Hosoya et al. in section 3.6.

3.2. Benchmark II: Size of the Solid Simulation Cell.

We began by investigating the mechanism(s) of cellulose pyrolysis at 327 °C using the smaller simulation cell in Figure 1 at 327 °C (denoted as “1unit”). The detailed picture and atomic numbering scheme of 1unit is shown in Figure 1. The simulation cell consists of one cellulose chain per sheet in the b direction and a total of 2 sheets per simulation cell. We used the following combination of two CVs: the distance between O₆–H_{O6} [$d(\text{O}_6\text{--H}_{\text{O6}})$], and the coordination number of the middle glycosidic O₁ with its bonded carbon atoms, C₁ and C₄.

This is denoted as CV set 1 listed in Table 3. As discussed in section 2.3, each atom in Table 3 is identified by the standard numbering of glucose used in the literature, cellulose chain number, and its position with respect to the middle glycosidic oxygen (away from the reader as positive and toward the reader as negative). For example, $^{4+}C_1$ in Table 3 means the C_1 atom on a glucose ring, on cellulose chain number 4, and the plus sign indicates that this atom is away from the reader with respect to middle oxygen O_1 . On performing a CPMD-metadynamics run with these CVs, at ~ 26.2 ps we observed a reaction involving exchange of hydrogen atoms among neighboring cellulose chains along the b direction. Since the atoms in the neighboring chain along the b direction are the periodic images of the cellulose chain itself, what we observed may be a spurious reaction mechanism that occurs due to the small size of the simulation cell. Since the simulation cell is thus deemed too small along the b axis, we extracted a bigger simulation cell with two chains along the b axis, denoted as "2unit." A detailed picture of this 2unit simulation cell and its atomic numbering scheme are shown in Figure 2.

We then performed CPMD-metadynamics calculations at 327°C for nearly 25 ps on the 2unitD simulation cell with a cutoff of 50 Ry using the CV set 1 listed in Table 3. As discussed in section 2, 2unitD involves a fixed-volume simulation cell with lattice parameters consistent with cellulose density at 327°C .⁸ This will be contrasted below with 2unitE, involving an expanded unit cell with a density appropriate to 600°C .⁸ At ~ 13.4 ps, we observed a rearrangement of hydrogens on oxygen atoms between neighboring chains shown as reaction scheme A in Table 2. Scheme A results from cooperative intrachain and interchain hydrogen-bond dynamics. The relatively high free-energy barrier for this process, 28 kcal/mol, is consistent with one of the O–O donor/acceptor distances (data not shown) being as large as 2.8–3.2 Å.^{88,89} A movie of the reaction mechanism is also provided in the Supporting Information.

Below we find that intrachain and interchain hydrogen bonding impact virtually all processes we harvested by CPMD. This also indicates that hydroxyl groups in cellulose can act as weak acids. This result motivated us to choose the coordination number of the glycosidic oxygen with respect to neighboring polar hydrogens as one of the CVs as discussed in section 2.4, imagining that the redistribution of these polar hydrogens may "catalyze" various processes in cellulose decomposition. In the rest of the work below we used the 2unit system as the size of the simulation cell.

3.3. Benchmark III: Solid Cellulose at 327°C . We performed several production-run CPMD-metadynamics simulations using a cutoff of 50 Ry to make these calculations computationally feasible as mentioned in section 2.2. We showed in section 3.1 that using a lower cutoff does not change the reaction mechanism; however, the lower cut off does produce a somewhat higher free-energy barrier. To determine the accuracy of this model chemistry, we performed CPMD-metadynamics simulations at 327°C on the 2unitD simulation cell with a cutoff of 50 Ry using CV set 4 in Table 3. We observed a depolymerization mechanism shown as reaction scheme D in Table 2. The glycosidic bond on the acetal carbon breaks at C_1 , and there is a hydrogen transfer from the C_2 carbon to yield a C_1 – C_2 double bond. This depolymerization mechanism has previously been observed by Assary and Curtiss, who modeled cellobiose as a surrogate for cellulose.⁵⁰

(We compare our computed barriers with those of Assary and Curtiss below in section 3.6.)

We plotted changes in distances between selected atoms during this CPMD-metadynamics run in Figure 5. Figure 5

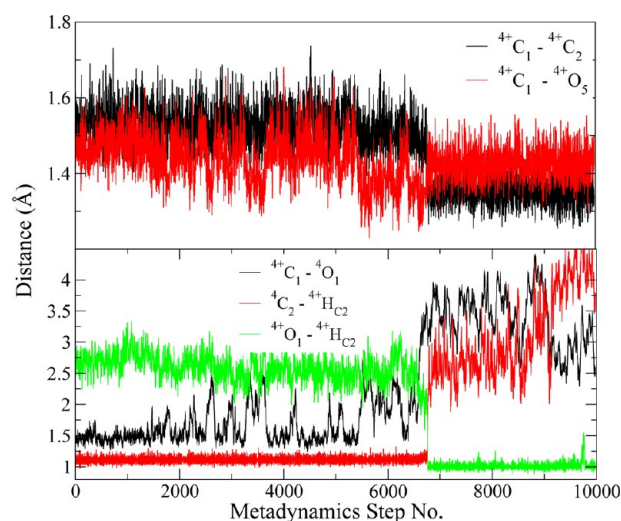


Figure 5. Changes in distances between selected atoms during CPMD-metadynamics run at 327°C for reaction scheme D shown in Table 2.

shows that this reaction proceeds with anchimeric assistance, i.e., with neighboring group participation.^{90,91} In particular, when O_1 breaks its bond with C_1 between metadynamics steps 5200 and 6800 (see Figure 5), the C_1 – O_5 bond length decreases from 1.46 ± 0.06 to 1.36 ± 0.05 Å for nearly 4 ps (>100 C–O vibrations), indicating the presence of a short-lived intermediate with C_1 – O_5 double-bond character facilitated by lone-pair donation from the neighboring O_5 "group". The undercoordinated O_1 atom is stabilized by both intra- and interchain hydrogen bonding with neighboring polar hydrogens as seen in the O_1 –H distances shown in Figure 6. Again, this suggests neighboring chains play an important role in determining cellulose pyrolysis chemistries (not shown in the simplified representation of the mechanism in Table 2). The

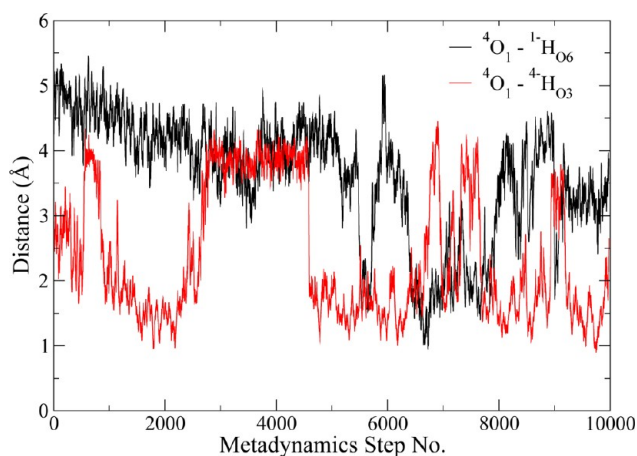


Figure 6. Changes in distances between selected atoms during CPMD-metadynamics run at 327°C for reaction scheme D shown in Table 2.

reaction is completed by transfer of $\text{H}_{\text{C}2}$ to O_1 and by C_1 forming a double bond with C_2 , all shown in Figure 5.

We found a free-energy barrier for this process of $\Delta F_{\text{CPMD-solid}}^\ddagger$ (327 °C) = 42 kcal/mol. To gauge the accuracy of this barrier and investigate the magnitude of condensed-phase effects, we performed comparable gas-phase calculations on constrained cellobiose with CPMD and Gaussian09, yielding $\Delta F_{\text{CPMD-gas}}^\ddagger$ (327 °C) and $\Delta G_{\text{GAU-gas}}^\ddagger$ (327 °C), respectively. The results of these benchmark calculations are shown in row 2 of Table 1. Using a cutoff of 70 Ry we found $\Delta F_{\text{CPMD-gas}}^\ddagger$ (327 °C) = 43 kcal/mol, apparently in excellent agreement with the 50 Ry solid result. However, this agreement likely arises from fortuitous cancellation of errors: the 50 Ry-solid calculation overestimates barriers, while the 70 Ry-gas calculation omits transition-state stabilization by hydrogen bonding (vide infra). Using BLYP/6-311G(d,p) within Gaussian09 gives $\Delta G_{\text{GAU-gas}}^\ddagger$ (327 °C) = 46 kcal/mol, while a single-point BLYP/cc-pvqz correction yields 45 kcal/mol. This once again suggests that the 70 Ry calculation gives accuracy comparable to the cc-pvqz basis set, although in this case the 6-311G(d,p) result is not far behind. Applying an MP2/6-311G(d,p) single-point correction yields $\Delta G_{\text{GAU-gas}}^\ddagger$ (327 °C) = 72 kcal/mol, which is 36% higher than the BLYP/6-311G(d,p) value. Rows 1 and 2 in Table 1 thus show that, for these reactions in cellulose pyrolysis, the BLYP density functional consistently underestimates these barriers by more than 30%.

Using a cutoff of 50 Ry we found a $\Delta F_{\text{CPMD-gas}}^\ddagger$ (327 °C) value of 51 kcal/mol, consistent with the results above showing that using a 50 Ry cutoff overestimates barriers by around 20%. Comparing this to the $\Delta F_{\text{CPMD-solid}}^\ddagger$ (327 °C) value of 42 kcal/mol shows that hydrogen bonding stabilizes the transition state by about 9 kcal/mol, which is completely consistent with the two hydrogen bonds observed in Figure 6, each worth about 5 kcal/mol.

Taken together, the results in this section paint a consistent picture of the importance of hydrogen bonding in cellulose chemistry and of the likely errors incurred by these solid CPMD-metadynamics calculations. In particular, we find that using the 50 Ry cutoff overestimates barriers by around 20%, while using the BLYP functional underestimates barriers by more than 30%. As such, although these are opposing trends, we conclude that our BLYP/50 Ry CPMD calculations likely *underestimate* true, condensed-phase barriers. We apply this qualitative conclusion below when comparing our results with experimental pyrolysis data.

3.4. Cellulose Decomposition Chemistry at 327 °C. We now report results of production CPMD-metadynamics runs that explore pyrolysis pathways at 327 °C using a cutoff of 50 Ry and various CV sets. Table 3 lists all the CV sets used in this work and the resulting free-energy barriers; Table 2 shows the reaction mechanisms that emerge from CPMD. Using CV sets 1 and 6 we found two distinct interchain rearrangements of hydrogen atoms, shown as reaction schemes A and G in Table 2, respectively. Again, this shows how neighboring chains play an important role in shuttling hydrogens during pyrolysis chemistry. Indeed, recent experiments have shown evidence of hydrogen exchange when deuterated glucose reacted with LGA under pyrolysis conditions.⁹²

We found ring contraction, shown as reaction scheme B in Table 2, to be the most common and the lowest-barrier reaction at 327 °C. We found this process to occur for CV sets 2, 5, 8, and 9. We observed a concerted mechanism from CPMD-metadynamics using CV set 8 (see Supporting

Information, Figure S7). We devised CV sets 2, 5, 8, and 9 to produce depolymerization at the glycosidic linkage by choosing one CV as the coordination number of the glycosidic oxygen with respect to its bonded carbons (see Supporting Information, Figure S7 shows that such glycosidic depolymerization is observed). In particular, at metadynamics step 6250 the $^4\text{C}_4$ – $^4\text{O}_1$ bond length changes from 1.55 ± 0.15 to 2.55 ± 0.16 Å (as shown in Figure S7, Supporting Information). The glycosidic oxygen ($^4\text{O}_1$) simultaneously forms a bond with another carbon on the ring ($^4\text{C}_5$), which is made possible through ring contraction. We computed various free-energy barriers for this process from different CV sets as shown in Table 3; CV set 9 gives the lowest free-energy barrier of 20 kcal/mol. These results echo the fact in many rare-event sampling methods that the computed value of a free-energy barrier depends on assumptions regarding the underlying reaction coordinate (or, in this case, the set of collective variables).⁹³

The other CV sets used at 327 °C are sets 7 and 17. CV set 7 was designed to produce a ring-opening reaction by including the coordination number of ring oxygen $^4\text{O}_5$ with its bonded ring carbons. Ring opening was indeed observed via a concerted mechanism shown in reaction scheme C in Table 2. CV set 17, on the other hand, yielded a precursor to LGA through an interesting bimolecular process. In particular, interchain exchange of hydrogens facilitated O_6 bridge formation with C_1 . This process occurs when $\text{H}_{\text{O}6}$ on cellulose chain 4 (i.e., $^4\text{H}_{\text{O}6}$) is transferred to O_6 on cellulose chain 1 (i.e., $^1\text{O}_6$). Further, $^1\text{O}_6$ transfers its bonded hydrogen to $^4\text{O}_1$, which in turn breaks its bond with $^4\text{C}_1$, and $^4\text{H}_{\text{O}6}$ forms a bond with $^4\text{C}_1$. A movie of this process is available in the Supporting Information. We computed a free-energy barrier of 69 kcal/mol for this reaction. This barrier is much higher than those found for the other processes at 327 °C discussed above, suggesting that formation of LGA is not kinetically favorable at this relatively low temperature. Experiments show that lower pyrolysis temperatures and higher residence times favor formation of char (solid) over tar (liquid).³ The present results hint that ring contraction (scheme B) may eventually lead to such “primary char.”

3.5. Cellulose Decomposition Chemistry at 600 °C.

Next, we performed CPMD-metadynamics simulations to investigate cellulose decomposition at 600 °C using the expanded 2unitE as the simulation cell. Below we also discuss CPMD-metadynamics at 600 °C using 2unitD as the simulation cell to investigate the effect of density on pyrolysis pathways. We note that 600 °C has been shown by Huber and co-workers to be the optimal temperature in *catalytic* fast pyrolysis of cellulose for maximizing the yield of aromatic fuels.⁵ Using a variety of CV sets, we found nascent decomposition routes to precursors of major pyrolysis products including LGA, HMF, and formic acid. We found that precursors to HMF and formic acid are formed directly from cellulose, supporting the previous computational findings by Mettler et al.³⁷ A complete list of the CV sets studied, and the barriers computed from CPMD-metadynamics, is provided in Table 3.

We applied several CV sets (sets 6, 14, 17, and 18) to model formation of a precursor to LGA, the major pyrolysis product. CV set 17 (mechanism Q in Table 2) yielded a low-barrier (36 kcal/mol) route to such a precursor, denoted pre-LGA. At about metadynamics step 1600, the $^4\text{C}_1$ – $^4\text{O}_5$ – $^4\text{C}_5$ – $^4\text{C}_4$ dihedral angle (data not shown) changes from 50° to –50°, indicating a conformational change from $^1\text{C}_4$ -chair to $^4\text{C}_1$ -chair,

echoing that seen for gas-phase methyl- β -D-glucoside in section 3.1. This conformational change is again left unresolved in the free-energy contour plot obtained from CPMD-metadynamics. However, the step can be observed in the movie of the process (see Supporting Information) and by monitoring this ${}^4\text{C}_1\text{--}{}^4\text{O}_5\text{--}{}^4\text{C}_5\text{--}{}^4\text{C}_4$ dihedral angle. Experiments support this facile conformational change by finding little difference in the kinetics of LGA formation as a function of the stereochemistry of the glycosidic linkage.⁹⁴

At about metadynamics step 2700, the $\text{C}_1\text{--O}_1$ bond breaks and the $\text{C}_1\text{--O}_5$ bond assumes a partial double-bond character (see Supporting Information, Figure S8, for changes in distances of selected atoms during this process). In particular, the $\text{C}_1\text{--O}_5$ bond length drops from 1.45 ± 0.07 to 1.35 ± 0.05 Å (see Supporting Information, Figure S8), representing another transition state stabilized by anchimeric assistance. The glycosidic oxygen (O_1) is again stabilized by hydrogen bonding as evidenced by the distances of O_1 with respect to ${}^4\text{H}_{\text{O}2}$ and ${}^4\text{H}_{\text{O}6}$ (see Supporting Information, Figure S8). The reaction completes at about metadynamics step 3300 with $\text{C}_1\text{--O}_5$ returning to its normal bond length and the $\text{C}_1\text{--O}_6$ bond forming to yield pre-LGA. A movie showing this reaction mechanism is available in the Supporting Information. Computed IR spectra of constrained gas-phase cellobiose and pre-LGA shows no clear spectroscopic signature which can mark formation of pre-LGA (see Supporting Information).

We also performed studies on several other CV sets to model depolymerization, ring-opening, and ring-fragmentation reactions as listed in Table 3 with reaction schemes shown in Table 2. Here we focus our discussion on mechanisms relevant to significant pyrolysis products or their precursors. Using CV set 3, we observed formation of a precursor to HMF, while CV set 16 yielded formic acid, both of which are formed in appreciable quantities during pyrolysis.³⁷ We found that formation of formic acid proceeds via an interesting four-membered ring (reaction scheme N), whereas pre-HMF is formed via a concerted mechanism whose transition state is stabilized by anchimeric assistance and nearby hydrogen bonding (reaction scheme K). Another product observed in this study is 2-hydroxy-1,3-propanedial (reaction scheme I), which is not observed as a pyrolysis product. However, 2-hydroxy-1,3-propanedial can further fragment to form glyxol and formaldehyde or glycoaldehyde and carbon monoxide, which are formed in appreciable quantities during pyrolysis. The computed free-energy barriers of these major products at 600 °C are in the order of pre-LGA (36 kcal/mol) < pre-HMF (49 kcal/mol) < formic acid (61 kcal/mol), suggesting that pre-LGA (and hence LGA itself) is kinetically favored at 600 °C.

We also performed studies to investigate the effect of density on pyrolysis pathways. We employed the simulation cell obtained at 327 °C (2unitD) and performed CPMD-metadynamics simulations at 600 °C using the same CV sets as discussed above. The 2unitD cell is 13% more dense than 2unitE. Results from these runs are summarized in Table 3. We could not find a low-barrier pathway leading to pre-LGA or any other major pyrolysis product. This suggests that LGA formation at high temperatures is facilitated by expansion of the cellulose matrix, perhaps giving more space for bicyclic ring formation. In general, this indicates that employing appropriate thermophysical constraints such as density is important for modeling solid-state reaction pathways.

3.6. Comparisons with Previous Calculations and Experiments. We now compare our CPMD-metadynamics

results with other CPMD simulations, previous gas-phase calculations, and experimental data.

Mettler et al. recently showed by CPMD simulations that solid cyclohexamylose, a surrogate for cellulose, converts to HMF and formic acid through homolytic cleavage of C–O bonds,³⁷ whereas we found concerted mechanisms to be more likely. Since no barriers were computed by Mettler et al., direct comparison to their results is not possible. To accelerate the decomposition reactions, Mettler et al. performed their CPMD simulations at much higher temperatures, in the range of 1700–2700 °C, while fast pyrolysis experiments are typically performed at 400–600 °C. Using such high temperatures may open new kinetic pathways not relevant at lower temperatures. Also, it was recently shown that the bond dissociation energy for homolytic cleavage of the C–O glycosidic bond is 91.8 kcal/mol for methyl- β -glucoside⁴⁴ (computed at the MP4/SDTQ model chemistry) and 79.1 kcal/mol for cellobiose [computed at B3LYP/6-31+G(d)].⁴⁹ The barriers computed herein are much lower than these homolytic dissociation energies, but such dissociation processes may become accessible in the 1700–2700 °C temperature range. Hosoya et al.⁴⁴ also showed that a concerted mechanism to LGA exhibits a much lower barrier than those from homolytic and heterolytic cleavage, recently corroborated by Mayes and Broadbelt⁵¹ on a larger system. All these results suggest that at the temperatures of fast pyrolysis concerted mechanisms are more likely than homolytic cleavage of C–O bonds.

For the gas-phase reaction of methyl- β -D-glucoside to LGA and methanol, Hosoya et al. report a concerted mechanism and a range of free-energy barriers at 327 °C. In particular, they find barriers in the range 47.7–61.1 kcal/mol from B3LYP/6-31+G(d), which grow to 55.7–69.8 kcal/mol using MP2/6-31+G(d).⁴⁴ Our gas-phase CPMD-metadynamics and Gaussian09 calculations agree with Hosoya et al. on the mechanism and yield free-energy barriers in the range 44–59 kcal/mol using BLYP with various basis sets and 68 kcal/mol using MP2/6-311G(d,p). This represents excellent agreement, which is not surprising considering we are modeling precisely the same system.

As discussed in the Introduction, Assary and Curtiss applied DFT to model the gas-phase reaction of cellobiose to LGA.⁵⁰ Their results suggest that cellobiose first depolymerizes to produce 1,2-dehydroglucopyranose, which further converts to LGA via 1,6-epoxide formation. For the first step (i.e., reaction scheme D in Table 2), Assary and Curtiss report gas-phase enthalpic barriers of 51.3 kcal/mol using B3LYP/6-31G++(2df,p) and 59.1 kcal/mol with corrections from MP2/6-311G++(3df,3pd). We modeled this first step in the gas phase with end-point-constrained cellobiose, finding bare electronic barriers of 54–55 kcal/mol using BLYP with various basis sets, which grows to 81 kcal/mol with MP2/6-311G(d,p). Two points about this comparison are noteworthy. First, our bare electronic barriers are consistently larger than those of Assary and Curtiss, likely because of the constraints we imposed on gas-phase cellobiose. Second, while the gas-phase calculations of Assary and Curtiss would suggest that cellulose converts to LGA through a multistep process, our solid cellulose CPMD-metadynamics simulations produce a bicyclic precursor to LGA in a one-step, concerted process with a free-energy barrier (36 kcal/mol) lower than any of those reported by Assary and Curtiss.

Direct comparison of the present calculations with experimental results is not currently possible because of the

challenges involved in both molecular modeling and experiments. Cellulose pyrolysis experiments may involve non-isothermal kinetics and limitations from heat and mass transfer.⁹⁵ Overall, the complexity of cellulose pyrolysis makes it extremely challenging to experimentally identify all participating reactions at the microscopic level. On the modeling side, the present calculations suffer from all of the above-mentioned quantum-chemical approximations, our calculations only proceed to *precursors* of major pyrolysis products, and we do not presently account for subsequent steps such as formation, diffusion, and vaporization of volatile organic compounds (e.g., LGA). Nonetheless, the present study opens the door to a preliminary comparison between experimental and computational results.

As discussed in the Introduction, although a wide range of experimental activation energies has been reported for cellulose pyrolysis,⁹ a much narrower range (45.4–47.8 kcal/mol) corresponds to fitted pre-exponential factors with physically plausible values of 10^{13} – 10^{14} s⁻¹,^{9,17–21} corresponding to molecular vibrational attempt frequencies. In the present study, we report a free-energy barrier of 36 kcal/mol for formation of a precursor to LGA, the major pyrolysis product. From our analysis of basis-set and level-of-theory errors, we conclude that this computed barrier underestimates the true barrier by as much as 15%, suggesting a corrected barrier around 41 kcal/mol. Considering that we ignore vaporization energetics, we expect to underestimate experimental apparent activation energies. Even this level of agreement is remarkable given the complexity of pyrolysis and the experimental sensitivity to the balance between char (solid) and tar (liquid) formation.⁹⁶

In the Introduction we distinguished “reversible active cellulose” below 260 °C which remains solid,⁹ from “liquid intermediate cellulose” above 260 °C, which likely requires depolymerization processes to facilitate melting. Our present results suggest that depolymerization via ring contraction (scheme B in Table 2) represents a key reaction in the transformation from reversible active cellulose to liquid intermediate cellulose. We furthermore suggest that formation of pre-LGA (scheme Q in Table 2) represents a central reaction in cellulose fast pyrolysis for temperatures in the range 400–600 °C.

4. CONCLUSION

We modeled decomposition reactions occurring in cellulose pyrolysis at 327 and 600 °C using Car–Parrinello molecular dynamics (CPMD) with rare reactive events accelerated with the metadynamics method. We found that a simulation cell consisting of four cellobiose residues periodically repeated in three dimensions is required to mimic the cellulose I β solid structure and reactivity. Classical NPT simulations were employed to generate initial conditions with plausible densities at the target pyrolysis temperatures. CPMD-metadynamics simulations were performed with various sets of collective variables, such as coordination numbers of the glycosidic oxygen to bonded carbons and also to nearby polar hydrogens. This computational procedure yielded a variety of chemical reactions such as depolymerization, fragmentation, ring opening, and ring contraction. These reactions yielded precursors to levoglucosan (denoted pre-LGA) and hydroxy-methylfurfural (pre-HMF) and also produced formic acid.

CPMD-metadynamics production runs were performed with the BLYP density functional using a planewave cutoff of 50 Ry (BLYP/50 Ry). Several gas-phase, benchmark calculations were

performed to gauge the basis set and level of theory errors in our BLYP/50 Ry production-run calculations. We found that using the 50 Ry cutoff consistently produced *higher* free-energy barriers than those from a cutoff of 70 Ry, which appears comparable to the accuracy of Dunning’s cc-pvqz basis set. We also found that using the BLYP functional consistently produced *lower* free-energy barriers than those from MP2 (same basis set) and that this level-of-theory effect is stronger than the basis-set effect. As such, we conclude that CPMD-metadynamics with BLYP/50 Ry produces free-energy barriers slightly lower than true, condensed-phase pyrolysis barriers.

At 327 °C, we found that ring contraction of the glucopyranose ring to the glucofuranose ring occurs with the lowest free-energy barrier (20 kcal/mol). At 600 °C, we found that a precursor to LGA (pre-LGA) forms with a free-energy barrier of 36 kcal/mol stabilized by anchimeric assistance and hydrogen bonding. Expansion of the cellulose matrix at 600 °C was found to be crucial for formation of pre-LGA. We found that free-energy barriers at 600 °C are in the order pre-LGA < pre-HMF < formic acid, suggesting why LGA is the kinetically favored product of fast cellulose pyrolysis.

Overall, our results suggest that depolymerization via ring contraction (scheme B in Table 2) represents a key reaction in the transformation from reversible active cellulose to liquid intermediate cellulose occurring near 260 °C. Moreover, we suggest that formation of the precursor to LGA (scheme Q in Table 2) represents an important initial reaction in cellulose fast pyrolysis for temperatures in the range 400–600 °C.

Future work is necessary to model formation, diffusion, and vaporization of volatile organic compounds during cellulose fast pyrolysis and determine the mechanisms of coke formation. Also important is the development of rational correlations between sets of collective variables used in metadynamics (and related rare-event methods) and the reactions they produce.

■ ASSOCIATED CONTENT

§ Supporting Information

Computational methods with all details; thermochemistry of representative cellulose pyrolysis reactions; changes in distances of selected atoms during CPMD-metadynamics run for reaction schemes B and Q; infrared spectra of constrained cellobiose and constrained pre-LGA; coordinates and energies of reactants, products, and transition states in Table 1; movies of important reaction mechanisms (reaction schemes A, K, I, N, and Q; methylglucoside to LGA; formation of pre-LGA from solid cellulose at 327 °C). This material is available free of charge via the Internet at <http://pubs.acs.org>.

■ AUTHOR INFORMATION

Corresponding Author

auerbach@chem.umass.edu

Present Addresses

[§]Material Research Laboratory, University of California, Santa Barbara, CA 93106

^{||}Department of Chemical Engineering, University of Wisconsin–Madison, Madison, WI 53706

Notes

The authors declare no competing financial interest.

■ ACKNOWLEDGMENTS

We thank the EFRI research team at UMass Amherst for stimulating discussions on cellulose pyrolysis. We also thank

Prof. Justin T. Fermann for enlightening discussions on quantum chemistry. This material is based upon work supported by the National Science Foundation under the Emerging Frontiers in Research and Innovation program (EFRI) 0937895.

REFERENCES

- (1) Huber, G. W.; Iborra, S.; Corma, A. *Chem. Rev.* **2006**, *106*, 4044–98.
- (2) Demirbas, A.; Arin, G. *Energy Sources* **2002**, *24*, 471–482.
- (3) Bridgwater, T. *Biomass Bioenergy* **2007**, *31*, Vii–Xviii.
- (4) Demirbas, M. F.; Balat, M. *J. Sci. Ind. Res.* **2007**, *66*, 797–804.
- (5) Carlson, T. R.; Vispute, T. P.; Huber, G. W. *ChemSusChem* **2008**, *1*, 397–400.
- (6) Bridgwater, A.; Meier, D.; Radlein, D. *Org. Geochem.* **1999**, *30*, 1479–1493.
- (7) Bridgwater, A. *Chem. Eng. J.* **2003**, *91*, 87–102.
- (8) Agarwal, V.; Huber, G. W.; Conner, W. C.; Auerbach, S. M. *J. Chem. Phys.* **2011**, *135*, 134506.
- (9) Lin, Y.-C.; Cho, J.; Tompsett, G. A.; Westmoreland, P. R.; Huber, G. W. *J. Phys. Chem. C* **2009**, *113*, 20097–20107.
- (10) Pérez, S.; Mazeau, K. In *Polysaccharides: Structural Diversity and Functional Versatility*, 2nd ed.; Dumitriu, S., Ed.; Marcel Dekker: New York, USA, 2005; Chapter 2, pp 41–68.
- (11) Car, R.; Parrinello, M. *Phys. Rev. Lett.* **1985**, *55*, 2471–2474.
- (12) Mohan, D.; Pittman, C. U.; Steele, P. H. *Energy Fuels* **2006**, *20*, 848–889.
- (13) Diblasi, C. *Prog. Energy Combust. Sci.* **2008**, *34*, 47–90.
- (14) Prakash, N.; Karunanithi, T. *J. Appl. Sci. Res.* **2008**, *4*, 1627–1636.
- (15) Prakash, N.; Karunanithi, T. *Asian J. Sci. Res.* **2009**, *2*, 1–27.
- (16) Vamvuka, D. *Int. J. Energy Res.* **2011**, *35*, 835–862.
- (17) Mamleev, V.; Bourbigot, S.; Yvon, J. *J. Anal. Appl. Pyrol.* **2007**, *80*, 141–150.
- (18) Bradbury, A. G. W.; Sakai, Y.; Shafizadeh, F. *J. Appl. Polym. Sci.* **1979**, *23*, 3271–3280.
- (19) Cooley, S.; Antal, M. J., Jr. *J. Anal. Appl. Pyrol.* **1988**, *14*, 149–161.
- (20) Antal, M. J.; Várhegyi, G.; Jakab, E. *Ind. Eng. Chem. Res.* **1998**, *37*, 1267–1275.
- (21) Banyasz, J. L.; Li, S.; Lyons-Hart, J. L.; Shafer, K. H. *J. Anal. Appl. Pyrol.* **2001**, *57*, 223–248.
- (22) Broido, A.; Evett, M.; Hodges, C. C. *Carbohydr. Res.* **1975**, *44*, 267–274.
- (23) Shafizadeh, F.; Bradbury, A. G. W. *J. Appl. Polym. Sci.* **1979**, *23*, 1431–1442.
- (24) Diebold, J. P. *Biomass Bioenergy* **1994**, *7*, 75–85.
- (25) Agrawal, R. K. *Can. J. Chem. Eng.* **1988**, *66*, 403–412.
- (26) Conesa, J. A.; Caballero, J. A.; Marcilla, A.; Font, R. *Thermochim. Acta* **1995**, *254*, 175–192.
- (27) Kilzer, F. J.; Broido, A. *Pyrolytics* **1965**, *2*, 9.
- (28) Várhegyi, G.; Jakab, E.; Antal, M. J., Jr. *Energy Fuels* **1994**, *8*, 1345–1352.
- (29) Alves, S. S.; Figueiredo, J. L. *J. Anal. Appl. Pyrol.* **1989**, *17*, 37–46.
- (30) Stamm, A. J. *Ind. Eng. Chem.* **1956**, *48*, 413–417.
- (31) Cho, J.; Davis, J. M.; Huber, G. W. *ChemSusChem* **2010**, *3*, 1162–5.
- (32) Agrawal, R. K. *Can. J. Chem. Eng.* **1988**, *66*, 413–418.
- (33) Mamleev, V.; Bourbigot, S.; Lebras, M.; Yvon, J. *J. Anal. Appl. Pyrol.* **2009**, *84*, 1–17.
- (34) Boutin, O.; Ferrer, M.; Lédé, J. *J. Anal. Appl. Pyrol.* **1998**, *47*, 13–31.
- (35) Liu, Q.; Wang, S.; Wang, K.; Guo, X.; Luo, Z.; Cen, K. *Acta Phys. Chim. Sin.* **2008**, *24*, 1957–1963.
- (36) Lédé, J.; Blanchard, F.; Boutin, O. *Fuel* **2002**, *81*, 1269–1279.
- (37) Mettler, M. S.; Mushrif, S. H.; Paulsen, A. D.; Javadekar, A. D.; Valchos, D. G.; Dauenhauer, P. J. *Energy Environ. Sci.* **2012**, *5*, 5414–5424.
- (38) Piskorz, J.; Radlein, D.; Scott, D. S. *J. Anal. Appl. Pyrol.* **1986**, *9*, 121–137.
- (39) Radlein, D.; Piskorz, J.; Scott, D. S. *J. Anal. Appl. Pyrol.* **1991**, *19*, 41–63.
- (40) Shen, D. K.; Gu, S. *Bioresour. Technol.* **2009**, *100*, 6496–504.
- (41) Geng, Z.; Zhang, M.; Yu, Y. *Fuel* **2012**, *93*, 92–98.
- (42) Nimlos, M. R.; Blanksby, S. J.; Qian, X.; Himmel, M. E.; Johnson, D. K. *J. Phys. Chem. A* **2006**, *110*, 6145–56.
- (43) Liu, C.; Huang, J.; Huang, X.; Li, H.; Zhang, Z. *Comput. Theor. Chem.* **2011**, *964*, 207–212.
- (44) Hosoya, T.; Nakao, Y.; Sato, H.; Kawamoto, H.; Sakaki, S. *J. Org. Chem.* **2009**, *74*, 6891–4.
- (45) Vasilu, M.; Guynn, K.; Dixon, D. A. *J. Phys. Chem. C* **2011**, *115*, 15686–15702.
- (46) Assary, R. S.; Curtiss, L. A. *Energy Fuels* **2012**, *26*, 1344–1352.
- (47) Abella, L.; Yamamoto, K.; Fukuda, K.; Nanbu, S.; Oikawa, N.; Morita, K.; Matsumoto, T. *Memoirs of the Faculty of Engineering, Kyushu University*; Faculty of Engineering: Kyushu University, Japan, 2006; Vol. 66, pp 147–168.
- (48) Nimlos, M. R.; Evans, R. J. *Renewable Energy* **2002**, *47*, 393–394.
- (49) Zhang, X.; Li, J.; Yang, W.; Blasiak, W. *Energy Fuels* **2011**, *25*, 3739–3746.
- (50) Assary, R. S.; Curtiss, L. A. *ChemCatChem* **2012**, *4*, 200–205.
- (51) Mayes, H. B.; Broadbelt, L. J. *J. Phys. Chem. A* **2012**, *116*, 7098–106.
- (52) Zhang, M.; Geng, Z.; Yu, Y. *Energy Fuels* **2011**, *25*, 2664–2670.
- (53) Dellago, C.; Bolhuis, P. G.; Geissler, P. L. *Adv. Chem. Phys.* **2002**, *123*, 1–78.
- (54) van Duin, A. C. T.; Dasgupta, S.; Lorant, F.; Goddard, W. A. *J. Phys. Chem. A* **2001**, *105*, 9396–9409.
- (55) Chenoweth, K.; van Duin, A. C. T.; Goddard, W. A. *J. Phys. Chem. A* **2008**, *112*, 1040–53.
- (56) Smith, K. D.; Stoliarov, S. I.; Nyden, M. R.; Westmoreland, P. R. *Mol. Simul.* **2007**, *33*, 361–368.
- (57) Tully, J. C. *Faraday Discuss.* **1998**, *110*, 407–419.
- (58) Saenger, W. α -Cyclodextrin Inclusion Complexes: Mechanism of Adduct Formation and Intramolecular Interactions. *Proceedings of the Eighth Jerusalem Symposium on Quantum Chemistry and Biochemistry*, Jerusalem, Israel, April 7–11, 1975; D. Reidel Pub. Co.: Dordrecht, 1975.
- (59) Saenger, W.; Jacob, J.; Gessler, K.; Steiner, T.; Hoffmann, D.; Sanbe, H.; Koizumi, K.; Smith, S. M.; Takaha, T. *Chem. Rev.* **1998**, *98*, 1787–1802.
- (60) Voter, A. *Phys. Rev. B* **1998**, *57*, R13985–R13988.
- (61) Voter, A. *Phys. Rev. Lett.* **1997**, *78*, 3908–3911.
- (62) Voter, A. F. *J. Chem. Phys.* **1997**, *106*, 4665–4677.
- (63) Sørensen, M. R.; Voter, A. F. *J. Chem. Phys.* **2000**, *112*, 9599–9606.
- (64) Laio, A.; Parrinello, M. *Proc. Natl. Acad. Sci. U.S.A.* **2002**, *99*, 12562–6.
- (65) Voter, A. F.; Montalenti, F.; Germann, T. C. *Annu. Rev. Mater. Res.* **2002**, *32*, 321–346.
- (66) van Der Spoel, D.; Lindahl, E.; Hess, B.; Groenhof, G.; Mark, A. E.; Berendsen, H. J. C. *J. Comput. Chem.* **2005**, *26*, 1701–18.
- (67) van der Spoel, D.; Lindahl, E.; Hess, B.; van Buuren, A. R.; Apol, E.; Meulenhoff, P. J.; Tieleman, D. P. J.; Sijbers, A. L. T. M.; Feenstra, K. A.; van Drunen, R.; Berendsen, H. J. C. *Gromacs User Manual*, version 4.0; 2005; www.gromacs.org.
- (68) Lins, R. D.; Hunenberger, P. H. *J. Comput. Chem.* **2005**, *26*, 1400–1412.
- (69) Kohn, W.; Sham, L. J. *Phys. Rev.* **1965**, *140*, A1133–A1138.
- (70) Hohenberg, P.; Kohn, W. *Phys. Rev.* **1964**, *136*, B864–B871.
- (71) CPMD: Car-Parrinello molecular dynamics; <http://www.cpmid.org/>. IBM Corp.: Stuttgart, 1990–2008; Copyright MPI für Festkörperforschung: Stuttgart, 1997–2001.

- (72) Becke, A. D. *Chem. Phys.* **1993**, *98*, 5648–5652.
- (73) Lee, C.; Yang, W.; Parr, R. G. *Phys. Rev. B* **1988**, *37*, 785–789.
- (74) Kittel, C. *Introduction to Solid State Physics*, 8th ed.; John Wiley & Sons, Inc.: New York, 2005.
- (75) Goedecker, S.; Teter, M.; Hutter, J. *Phys. Rev. B* **1996**, *54*, 1703–1710.
- (76) Dong, H.; Nimlos, M. R.; Himmel, M. E.; Johnson, D. K.; Qian, X. *J. Phys. Chem. A* **2009**, *113*, 8577–85.
- (77) Qian, X.; Johnson, D. K.; Himmel, M. E.; Nimlos, M. R. *Carbohydr. Res.* **2010**, *345*, 1945–51.
- (78) Liu, D.; Nimlos, M. R.; Johnson, D. K.; Himmel, M. E.; Qian, X. *J. Phys. Chem. A* **2010**, *114*, 12936–44.
- (79) Frisch, M. J.; Trucks, G. W.; Schlegel, H. B.; Scuseria, G. E.; Robb, M. A.; Cheeseman, J. R.; Scalmani, G.; Barone, V.; Mennucci, B.; Petersson, G. A.; Nakatsuji, H.; Caricato, M.; Li, X.; Hratchian, H. P.; Izmaylov, A. F.; Bloino, J.; Zheng, G.; Sonnenberg, J. L.; Hada, M.; Ehara, M.; Toyota, K.; Fukuda, R.; Hasegawa, J.; Ishida, M.; Nakajima, T.; Honda, Y.; Kitao, O.; Nakai, H.; Vreven, T.; Montgomery, J. A., Jr.; Peralta, J. E.; Ogliaro, F.; Bearpark, M.; Heyd, J. J.; Brothers, E.; Kudin, K. N.; Staroverov, V. N.; Kobayashi, R.; Normand, J.; Raghavachari, K.; Rendell, A.; Burant, J. C.; Iyengar, S. S.; Tomasi, J.; Cossi, M.; Rega, N.; Millam, J. M.; Klene, M.; Knox, J. E.; Cross, J. B.; Bakken, V.; Adamo, C.; Jaramillo, J.; Gomperts, R.; Stratmann, R. E.; Yazyev, O.; Austin, A. J.; Cammi, R.; Pomelli, C.; Ochterski, J. W.; Martin, R. L.; Morokuma, K.; Zakrzewski, V. G.; Voth, G. A.; Salvador, P.; Dannenberg, J. J.; Dapprich, S.; Daniels, A. D.; Farkas, Ö.; Foresman, J. B.; Ortiz, J. V.; Cioslowski, J.; Fox, D. J. *Gaussian 09*, Revision A.1; Gaussian Inc.: Wallingford CT, 2009.
- (80) Dunning, T. H., Jr. *J. Chem. Phys.* **1989**, *90*, 1007.
- (81) Kendall, R. A.; Dunning, T. H.; Harrison, R. J. *J. Chem. Phys.* **1992**, *96*, 6796.
- (82) Woon, D. E.; Dunning, T. H. *J. Chem. Phys.* **1993**, *98*, 1358.
- (83) Ensing, B.; De Vivo, M.; Liu, Z.; Moore, P.; Klein, M. L. *Acc. Chem. Res.* **2006**, *39*, 73–81.
- (84) Laio, A.; Gervasio, F. L. *Rep. Prog. Phys.* **2008**, *71*, 126601.
- (85) Barducci, A.; Bonomi, M.; Parrinello, M. *Adv. Rev.* **2011**, *00*, 1–18.
- (86) Andersson, M.; Uvdal, P. *J. Phys. Chem. A* **2005**, *109*, 2937–2941.
- (87) Fermann, J. T.; Blanco, C.; Auerbach, S. M. *J. Chem. Phys.* **2000**, *112*, 6779.
- (88) Chan, B.; DelBene, J. E.; Radom, L. *Mol. Phys.* **2009**, *107*, 1095–1105.
- (89) Viswanathan, U.; Basak, D.; Venkataraman, D.; Fermann, J. T.; Auerbach, S. M. *J. Phys. Chem. A* **2011**, *115*, 5423–5434.
- (90) Smith, M. B.; March, J. *March's Advanced Organic Chemistry: Reactions, Mechanisms, and Structure*, 6th ed.; John Wiley & Sons, Inc.: New Jersey, 2007.
- (91) Morrison, R. T.; Boyd, R. N. *Organic Chemistry*, 5th ed.; Allyn and Bacon, Inc.: Boston, MA, 1987.
- (92) Mettler, M. S.; Paulsen, A. D.; Vlachos, D. G.; Dauenhauer, P. J. *Energy Environ. Sci.* **2012**, *5*, 7864–7868.
- (93) Truhlar, D. G.; Garrett, B. C. *Annu. Rev. Phys. Chem.* **1984**, *35*, 159–189.
- (94) Ponder, G. R.; Richards, G. N.; Stevenson, T. T. *J. Anal. Appl. Pyrol.* **1992**, *22*, 217–229.
- (95) Mettler, M. S.; Vlachos, D. G.; Dauenhauer, P. J. *Energy Environ. Sci.* **2012**, *5*, 7797–7809.
- (96) Milosavljevic, I.; Oja, V.; Suuberg, E. M. *Ind. Eng. Chem. Res.* **1996**, *35*, 653–662.